

# Morphological Exploration of Shape Spaces

Jesús Angulo and Fernand Meyer

CMM-Centre de Morphologie Mathématique, Mathématiques et Systèmes, MINES  
Paristech; 35, rue Saint Honoré, 77305 Fontainebleau Cedex, France  
`jesus.angulo@ensmp.fr`, `fernand.meyer@ensmp.fr`

**Abstract.** The aim of this paper is to propose efficient tools for analysing shape families using morphological operators. The developments include the definition of shape statistics (mean and variance of shapes, modes of shape variation) and the interpolation/extrapolation in shape geodesic paths. The main required ingredients for the operators and the algorithms here introduced are well known in mathematical morphology such as the median set, the watershed on distance functions or the interpolation function. In addition, the projection of shapes in spaces with reduced dimensions using PCA or ISOMAP techniques permits to apply morphological interpolation techniques in shape manifolds.

## 1 Introduction

Let  $\mathcal{X} = \{X_1, X_2, \dots, X_N\} = \{X_i\}_{i=1}^N$  be a family (or collection) of  $N$  shapes, where  $X_i \in \mathcal{P}(E)$  represents the set (or binary image) of the shape  $i$ , and the support space  $E$  is a nonempty set. Typically for the digital 2D images  $E \subset \mathbb{Z}^2$ . The set  $X_i$  is a compact set (and typically a closed simply connected set). The family  $\mathcal{X}$  can be considered as a random variable of shape, where  $X_i$  represents a realization of this random variable. The family may also be viewed as defined in a shape space, where  $\mathcal{X}$  is modelled as a low dimensional manifold embedded in a higher-dimensional space. The aim of this paper is to propose efficient tools for analysing shape families using morphological operators. This kind of analysis includes the definition of shape statistics (mean and variance of shape, modes of variation of shape) and the interpolation/extrapolation in shape manifolds or in shape geodesic paths.

Statistical theory of shapes has been studied by Kendall [9], representing the shapes as a finite number of salient points; and by Grenander [6], considering the shapes as points on some infinite-dimensional differentiable manifold, under the actions of Lie groups. More in relation with our study, Klassen *et al.* [10] proposed statistical shape analysis and shape interpolation by differential geometry methods, where the shapes are represented by curvature functions. Whitaker [16] proposed a method for image blending by progressive minimisation of a difference metric in a variational framework (i.e., a pair of coupled nonlinear PDE), where the metric is based on computing the distance between level-set shapes (distance function for binary images). Charpiat *et al.* [3] and Etyngier *et al.* [5] formalised the problem by optimizing mappings based on the Hausdorff metric and the signed distance functions.

**Background notions.** The main required ingredients for the operators and the algorithms introduced here are well known in mathematical morphology.

Let  $E$  be a metric space equipped with a distance  $d_M : E \times E \rightarrow \mathbb{R}_+$ , and let  $\mathcal{K}'$  be the class of the non empty compact sets of  $E$ . The *distance of point  $x$  to set  $Y$*  is defined as  $d_M(x, Y) = \inf\{d_M(x, y), y \in Y\}$ ,  $x \in E$  and  $Y \in \mathcal{K}'$ . Then, the *distance function of set  $X$*  according to metric  $d_M$  is the mapping  $\Delta_M X : E \rightarrow \mathbb{R}_+$ , such that

$$\Delta_M X(x) = d_M(x, X^c) = \inf\{\|x, y\|_M : y \in X^c\}.$$

We also use in this study the notion of distance between two shapes. Given two sets  $X, Y \in \mathcal{K}'$ , the most basic mapping  $\mathcal{K}' \times \mathcal{K}' \rightarrow \mathbb{R}_+$  to compare two sets is their *Euclidean distance*, i.e.,  $d_E(X, Y) = \sum_{\mathbf{x} \in E} 1_{\mathbf{x} \in [(X \cup Y) \setminus (X \cap Y)]}$ . Classically, it is considered most useful in practice the distance associated to the *Jacquard coefficient*:

$$d_J(X, Y) = 1 - \frac{\sum_{\mathbf{x} \in E} 1_{\mathbf{x} \in (X \cap Y)}}{\sum_{\mathbf{x} \in E} 1_{\mathbf{x} \in (X \cup Y)}} = \frac{\sum_{\mathbf{x} \in E} 1_{\mathbf{x} \in X \Delta Y}}{\sum_{\mathbf{x} \in E} 1_{\mathbf{x} \in (X \cup Y)}},$$

where  $X \Delta Y = [(X \cup Y) \setminus (X \cap Y)]$ . Furthermore, the natural metric to compare spatial shapes is the Hausdorff distance:

$$d_H(X, Y) = \max \left\{ \sup_{x \in X} d(x, Y) ; \sup_{y \in Y} d(y, X) \right\}.$$

The *Hausdorff distance* can also be expressed by means of the dilations by the balls of space  $E$  [14]:

$$d_H(X, Y) = \inf \{ \lambda : X \subseteq \delta_\lambda(Y); Y \subseteq \delta_\lambda(X) \},$$

with  $\delta_\lambda(X)$  being the dilation of  $X \in \mathcal{K}'$  by a radius of size  $\lambda \in \mathbb{R}_+$ :  $\delta_\lambda(X) = \cup \{B_\lambda(x), x \in X\}$ , where  $B_\lambda(x)$  stands for the compact ball of centre  $x$  and of radius  $\lambda$ .

The theory of morphological interpolation was introduced in [11,2,14]. In particular, the *interpolation distance function* [11],

$$\text{interp}_{X \rightarrow Y}(x) = \frac{d_X^Y(x)}{d_X^Y(x) + d_Y^X(x)},$$

and the *morphological median set* [2]:

$$m(X, Y) = Y \Delta \{x : \text{interp}_{X \rightarrow Y}(x) \leq 0.5\},$$

will be frequently used below. The distance  $d_X^Y(x) : E \times E \rightarrow \mathbb{R}_+$  to set  $X$  in set  $Y$  is defined as [13]:

$$d_X^Y(x) = n \quad \text{if} \quad (\varepsilon_X^n(Y) = 0 \quad \text{and} \quad \varepsilon_X^{n-1}(Y) = 1),$$

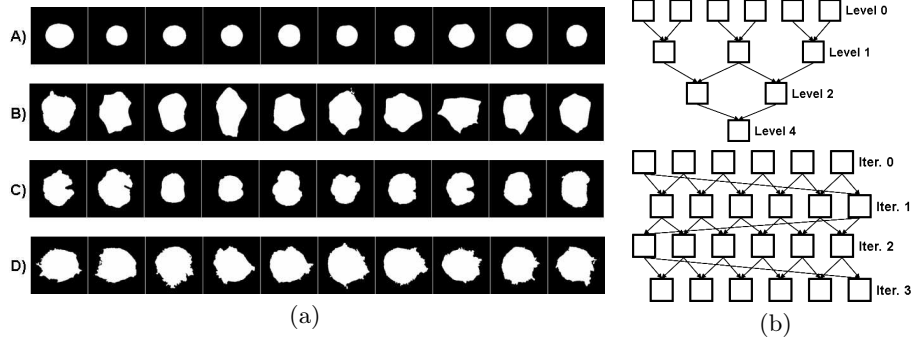


**Fig. 1.** (a) Four population of cells, each one representing a spatially equivalent shape family  $\mathcal{X}$ . (b) Two approaches for computing the mean shape using the median set: top, merger algorithm and bottom, iterative algorithm.

where  $\varepsilon_X^1(Y) = X \cap \delta_1(X \cap Y)$  for points on  $Y \subseteq X$ ,  $\varepsilon_X^1(Y) = X \cup \varepsilon_1(X \cup Y)$  for points on  $X \subseteq Y$ ; and  $\varepsilon_X^n(Y) = \varepsilon_X^1 \varepsilon_X^{n-1}(Y)$ .

Shape analysis makes no sense without a renormalisation of shapes. We only consider *spatially equivalent shape families*: two shapes will be considered as equivalent if there exists a rotation and a translation transforming one shape in the other. In practice, the mass center and the angle of orientation of principal axis are obtained by computing the second order inertia moments. Then the shapes are aligned and rotated to impose the same centroid and the same principal axis of variation, see in Fig. 1(a) four examples of spatially equivalent shape families. Other algorithms of centring and orientation can be considered, e.g. embedding which maximises the intersection between the sets [7], or which minimises the Hausdorff distance between the sets [14].

## 2 Shape Statistics

Let us start with the basics of shape statistics, the mean shape  $\mu_{\mathcal{X}}$  and the variance of shape  $\sigma_{\mathcal{X}}^2$  from a shape family  $\mathcal{X}$ . These basic statistics are needed for instance to build prototypes or shape priors in model-based image segmentation or to define primary grains for Boolean modelling and simulation. We describe and compare 3 different methods.

### 2.1 Computation of Mean Shapes

**Approach based on the median set  $\mu_{\mathcal{X}}^{ms}$ .** The morphological median set is defined only for two sets, i.e.,  $m(X_1, X_2)$ . The extension to  $N$  sets requires consequently the combination of successive median sets. Fig. 1(b) illustrates two different cascaded median set operators to compute  $\mu_{\mathcal{X}}^{ms}$ . The merger algorithm leads sequentially to a single final shape, whereas the iterative algorithm is applied until that the cumulated distance between sets is lower than

a fixed threshold (i.e., convergence to the mean set). Both algorithms depend on the ordering of the operators since the median set is not associative, i.e.,  $m(m(X_1, X_2), X_3) \neq m(X_1, m(X_2, X_3))$ . Empirical observations show that the iterative algorithm depends less upon the ordering of the sets and converges after a few iterations, however the merger algorithm requires less computation and at the end the results are quite similar.

**Extrinsic mean by thresholding the sum of distance functions  $\mu_{\mathcal{X}}^{thres}$ .**

The sum of the distance functions of the sets in  $\mathcal{X}$  has been widely used in the literature to build the theory of averaging shapes [4,1], although the associated algorithms to estimate the mean shapes are often inefficient. Inspired by the work [1], we propose to use both the inner and outer distance functions to estimate two extrinsic means, where the inner distance function of the family is  $\Delta\mathcal{X}(x) = \sum_i^N \Delta X_i(x)$  and the outer distance function is  $\Delta\mathcal{X}^c(x) = \sum_i^N \Delta X_i^c(x)$ . The algorithm aims at computing an optimal level set in  $\Delta\mathcal{X}(x)$ .

Let  $X^u \in \mathcal{P}(E)$  be the set obtained by thresholding the inner distance function at value  $u$ , i.e.,

$$X^u = \{x \in E : \Delta\mathcal{X}(x) \geq u\}, \quad u \in [0, \max(\Delta\mathcal{X}(x))].$$

We define the cumulative distance of shape family  $\mathcal{X}$  to set  $X^u$  by

$$D_{\Delta\mathcal{X}(x)}(u) = \sum_i^N d_M(X_i, X^u),$$

where  $d_M(\cdot, \cdot)$  is the distance between the two sets. Then the inner extrinsic mean is defined as

$$\mu_{\mathcal{X}}^{inner} = \arg_u \min D_{\Delta\mathcal{X}(x)}(u),$$

this minimization problem can be solved by an exhaustive search algorithm (i.e., discretization of  $\Delta\mathcal{X}(x)$  in  $K$  thresholded sets and selection of the minimum). A similar outer extrinsic mean  $\mu_{\mathcal{X}}^{outer}$  can be defined from optimal thresholding on function  $D_{\Delta\mathcal{X}^c(x)}(u)$ . The associated extrinsic mean shape  $\mu_{\mathcal{X}}^{thres}$  is then defined as the median set between  $\mu_{\mathcal{X}}^{inner}$  and  $\mu_{\mathcal{X}}^{outer}$ . Fig. 2(a) gives an example of the various elements for an example. An important parameter of this algorithm is the distance  $d_M(\cdot, \cdot)$ . We have compared the performance of both the Jacquard distance and the Hausdorff distance: it appears that the obtained mean shapes are more interesting when the Jacquard distance is chosen.

**Locally optimal mean by watershed of sum of squared distance functions  $\mu_{\mathcal{X}}^{wshed}$ .**

The previous approach presents two main limitations: i) the inner and outer distance functions are used separately, ii) the obtained mean shape is optimal only for a constant level set. A more original and powerful technique to exploit the sum of distance functions is based on the classical definition of the mean  $\mu$  of  $N$  samples:  $\mu$  is the value such that  $\sum_i^N (\mu - x_i)^2$  is minimal, which leads to  $\sum_i^N (\mu - x_i) = 0$  and consequently to  $N\mu = \sum_i^N x_i$ . In the extension

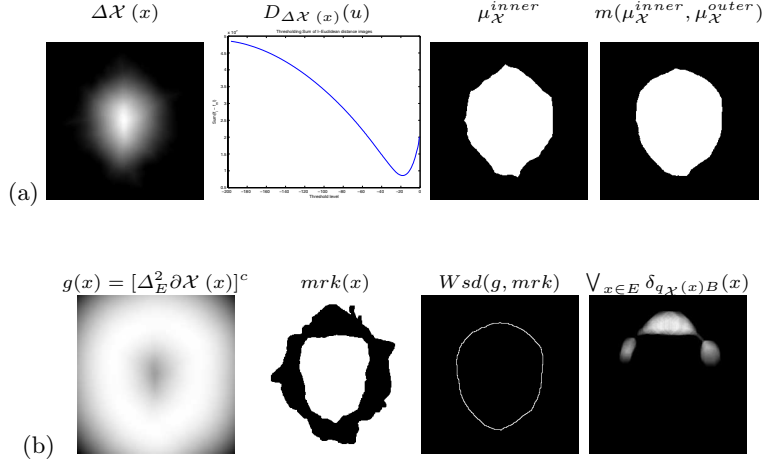


**Fig. 2.** (a) Computation of extrinsic mean by thresholding the sum of distance functions. (b) Computation of locally optimal mean by watershed of sum of squared distance functions.  $\mathcal{X}$  is the population B) of Fig. 1(a), where the last image represents an intermediate step of the quench function reconstruction.

to the case of the shape family  $\mathcal{X}$ , we start by constructing the sum of distance functions to the frontier sets  $\partial X_i$  using the squared Euclidean distance, i.e.,

$$\Delta_E^2 \partial\mathcal{X}(x) = \sum_i^N \Delta_E^2 \partial X_i(x),$$

which takes simultaneously the inner/outer distance functions. The locally minimal contour of  $\Delta_E^2 \partial\mathcal{X}(x)$  corresponds, by definition, to the mean shape.

This optimal contour can be easily obtained by computing the watershed line of the inverse of this distance function, i.e.,

$$\partial\mu_{\mathcal{X}}^{wshed} = Wshed([\Delta_E^2 \partial\mathcal{X}(x)]^c, mrk(x)),$$

where the marker function is  $mrk(x) = \varepsilon_B(mrk^{in}(x)) \cup \varepsilon_B(mrk^{out}(x))$ , with  $mrk^{in} = \{\bigcap_i X_i\}$  and  $mrk^{out} = [\{\bigcup_i X_i\}]^c$ . Fig. 2(b) depicts an example of the algorithm. Replacing the  $L^2$  norm by the  $L^1$  norm and calculating the watershed from the inverse of  $\Delta_E \partial\mathcal{X}(x)$  leads to the contour of the median shape of the family.

We have compared the three approaches  $\mu_{\mathcal{X}}^{ms}$ ,  $\mu_{\mathcal{X}}^{thres}$  and  $\mu_{\mathcal{X}}^{wshed}$  for computing mean shape from the same family. The three algorithms yield very similar results. However the last method, summing the squared distance function to the contours and extracting its thalweg line (watershed of the inverse function) is by far the most efficient. Moreover, as we show below, it is also useful to compute the shape variance.

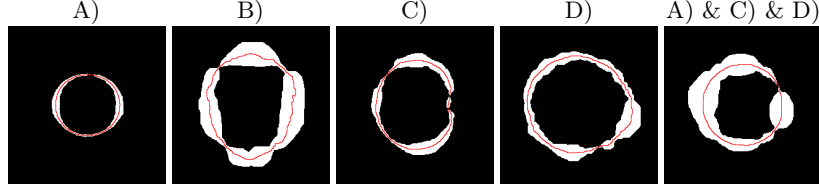


**Fig. 3.** Mean shapes  $\partial\mu_{\mathcal{X}}^{wshed}$  (in red) and std. dev. of shape  $\sigma_{\mathcal{X}}$  (in white) for the populations of cells of Fig. 1(a).

## 2.2 Variance of a Shape Family

Having defined a mean shape, we can now explore the computation of the variance of a shape family. In fact, it is more interesting, for the purpose of representation as an image, to obtain the standard deviation  $\sigma_{\mathcal{X}}$ .

If we remind that the variance of a set of points is  $\sigma^2 = 1/N \sum_i^N (\mu - x_i)^2$ , it is evident that the variance can be easily computed from  $\Delta_E^2 \partial\mathcal{X}(x)$ . More precisely, starting from the squared quench function of the family of shapes  $\mathcal{X}$ , which is defined as:

$$q_{\mathcal{X}}^2(x) = \begin{cases} (1/N) \cdot \Delta_E^2 \partial\mathcal{X}(x) & \text{if } x \in \partial\mu_{\mathcal{X}}^{wshed} \\ 0 & \text{if } x \in [\partial\mu_{\mathcal{X}}^{wshed}]^c \end{cases}$$

then, the image representation of the standard deviation of shape is obtained by the *reconstruction* of the quench function:

$$\sigma_{\mathcal{X}} = \bigvee_{x \in E} \delta_{q_{\mathcal{X}}(x)}(x).$$

In Fig. 3 are given the mean shape and the std. dev. of shape for the populations of cells of Fig. 1(a).

The notion of shape variance can be also obtained using alternative algorithms. For instance, after computing the distance of each shape  $X_i$  to their mean  $\mu_{\mathcal{X}}$ , i.e.,  $d_{\mu_{\mathcal{X}}}^{X_i}(x)$ , the variance on the frontier of the mean shape,  $\partial\mu_{\mathcal{X}}$ , can be approached by  $1/N \sum_i^N (d_{\mu_{\mathcal{X}}}^{X_i})^2$ .

## 3 Linear Methods for Dimensionality Reduction: Eigenshapes, Modes of Shape Variation

The computation of the mean shape (and variance of shape) has real sense only in the case of homogenous shape families since on collections of very heterogeneous shapes, the mean tends to be a circle. The application of standard techniques of multivariate data analysis can help the exploration of shape families (to determine the homogenous subfamilies) and their representation in spaces

of reduced dimension. The most classical approach is the principal component analysis (PCA) [8].

The basic idea is to represent the sets as vectors:  $X_i \in \mathcal{P}(E) \rightarrow \mathbf{x}_i \in \mathbb{R}^D$  ( $D$  is the cardinal of discrete space  $E$ ), thus the shape family is now given by the following matrix of data  $\mathbf{X} = [\mathbf{x}_1 \ \mathbf{x}_2 \ \cdots \ \mathbf{x}_N]$ . The covariance matrix of centred data:  $\mathbf{C}_{\mathbf{X}\mathbf{X}} = \text{cov}(\hat{\mathbf{X}})$ , where  $\hat{\mathbf{X}} = \mathbf{X} - \bar{\mathbf{X}}$  (if the average  $\bar{\mathbf{X}}$  is not subtracted, the average will appear as the first principal component) summarizes the variability of the family, analysed by solving the following spectral problem  $\mathbf{C}_{\mathbf{X}\mathbf{X}}\mathbf{w} = \lambda\mathbf{w}$ , whose eigendecomposition leads to  $[\Lambda, \mathbf{W}] = \text{eig}(\mathbf{C}_{\mathbf{X}\mathbf{X}})$ , where  $\Lambda$  is the diagonal matrix of different eigenvalues  $\lambda_j$  and  $\mathbf{W}$  is the matrix of the associated eigenvectors  $\mathbf{w}_j$ . The relative value of  $\lambda_j$  (i.e., the variance of shape explained by the axis  $j$ ) is used to determine the number of significant dimensions  $K$ .

Fig. 4 illustrates the method. First of all, it is possible to produce an image representation of the  $K$  first shape modes  $\{\mathbf{v}_j\}_{j=1}^K$ :  $\mathbf{v}_j = \hat{\mathbf{X}}\mathbf{w}_j$ . The corresponding images of the eigenvectors,  $V_j(x)$ , are the eigenshapes which correspond to the principal modes of shape variation (see Fig. 4(a)). In addition, the  $N$  values of each eigenvector correspond to the projection of each shape onto this vector (see Fig. 4(a)). This can be used typically for shape clustering (i.e., unsupervised classification in shape space in order to identify sub-families of shapes). Another application is the computation of an intrinsic mean shape as follows:

$$\hat{\nu}_{\mathcal{X}} = \arg_{\mathbf{s}_{k \in 1,2,\dots,N}} \min \sum_{i=1}^N \left( \sum_{j=1}^K (\mathbf{s}_j(i) - \mathbf{s}_j(k))^2 \right),$$

where  $\mathbf{s}_j(i) = \mathbf{W}^T \mathbf{x}_i$ , i.e.,  $\hat{\nu}_{\mathcal{X}}$  is the shape which minimises his cumulated distance to the other shapes in the PCA space (see Fig. 4(b)).

PCA has already been applied to shape analysis [7], but the exploitation of the eigenshapes has not yet considered in detail. One of the basic objectives is to decompose the eigenshapes into binary images representing the orthogonal modes of variation. As we observe in the eigenshapes images  $V_j(x)$ , the modes are differentiated by positive/negative structures on a reference intensity. Using the classical close-holes operator, we can decompose both phases into two different images:

$$V_{j\downarrow}(x) = [\text{CloseHoles}(V_j^c(x))]^c ; V_{j\uparrow} = [\text{CloseHoles}(V_j(x))].$$

The objective is to construct two closed binary shapes from  $V_{j\downarrow}$  and  $V_{j\uparrow}$ , but as we can observe in Fig. 4(c), the “modes of shape variation” require an additional “average shape”  $V_0(x)$ , which is obtained from the image of the average:  $\bar{\mathbf{X}} \rightarrow V_0(x)$ . The gradient of each image  $V_{j\downarrow}$  and  $V_{j\uparrow}$  is combined by sum with the gradient of the average image, i.e.,  $g_0(x) = \delta_1(V_0)(x) - \varepsilon_1(V_0)(x)$ . Hence, the two phases of mode of variation  $j$  can be now segmented with the watershed transformation as follows:

$$\text{Wshed}(\hat{g}_{j\downarrow}(x), \text{mrk}(x)) ; \text{Wshed}(\hat{g}_{j\uparrow}(x), \text{mrk}(x)),$$

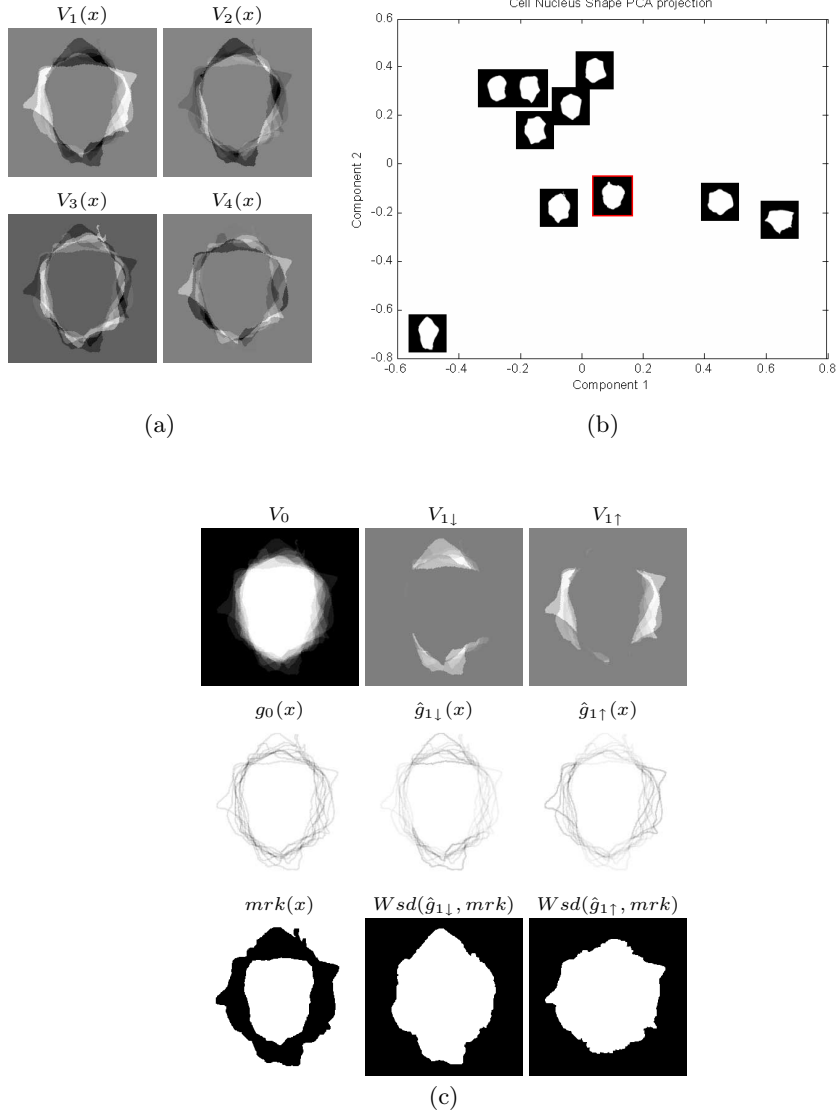


**Fig. 4.** Shape analysis using PCA of family  $\mathcal{X}$  (population B) of Fig. 1(a): (a) Four first eigenshapes. (b) Projection of shapes on the two first components (in red, intrinsic mean shape). (c) Morphological segmentation of modes of variation from the first eigenshape (see the text for full details).

where  $\hat{g}_{j\downarrow}(x) = g_{j\downarrow}(x) + g_0(x)$  with  $\hat{g}_{j\downarrow}(x) = \delta_1(V_{j\downarrow})(x) - \varepsilon_1(V_{j\downarrow})(x)$ . The obtained images for the example are also given in Fig. 4(c).

Morphological interpolation does not always a good job if two shapes are too dissimilar; PCA can then be used as a useful preprocessing: the shapes  $X$  and  $Y$



to be interpolated are first projected onto the different  $K$  principal components produced by PCA ; the projections are then interpolated separately. Finally, the  $K$  interpolated shapes are recombined linearly in order to obtain the final shape.

#### 4 Isometric Shape Spaces and Geodesic Shape Interpolation

PCA is based on the covariance matrix of the shape family, which corresponds to consider a dimensionality reduction using the Euclidean distance of shapes. A lot of effort has been paid in recent years to introduce nonlinear dimensionality reduction techniques compatible with other distances between the points of the space. Particularly interesting for our purposes is the isometric feature mapping (ISOMAP) [15]. It is a method for estimating the intrinsic geometry of a data manifold based on a rough positioning of the neighbours of each data point on the manifold. More precisely, it is a low-dimensional embedding method based on geodesic distances on a weighted neighbourhood graph, which is then reduced by multidimensional scaling (MDS). ISOMAP depends on being able to choose the neighbourhood size (k-nearest neighbours graph) and on a distance to compare each pair of points (weights of edges of graph). This weighted graph defines the connectivity of each data point via its nearest neighbours in the high-dimensional space. The precise algorithm for ISOMAP is described in [15].

In Fig. 5(a) is given the two-dimensional ISOMAP embedding (with the neighbourhood graph) for the four populations of Fig. 1(a). We have compared various distances to weight the graph, and again the Jacquard distance outperforms the Hausdorff distance in our examples. Compared to the PCA projection of shape families, the ISOMAP embedding allows to define geodesic paths between the shapes, and in addition, the shortest path distances in the neighbourhood graph are preserved in the two dimensional embedding recovered by ISOMAP. This property is specially useful for the interpolation of shapes in the family  $\mathcal{X}$  (see Fig. 5(b)). For instance, given two shapes  $X_i$  and  $X_j$ , an Euclidean shape path

$$[X^0 = X_i, X^P = X_j]$$

of  $P - 1$  intermediate points  $X^k$  is classically obtained by thresholding the interpolating function  $\text{interp}_{X^0}^{X^P}(x)$  at values  $\lambda = (1/P) \cdot k$ , with  $k = 1, 2, \dots, P - 1$ . Now, using the ISOMAP graph, we can define the geodesic shape path

$$\Pi_{P+1}(X_i, X_j) = (X^0 = X_i, X^1, \dots, X^P = X_j),$$

which includes the  $Q$  shapes of the family  $\mathcal{X}$  belonging to the path. The remaining  $(P - Q - 1)$  shapes are computed by the interpolation function according to their respective geodesic distance, i.e., the number of intermediate shapes between two successive shapes  $X_n$  and  $X_m \in \Pi_{P+1}(X_i, X_j)$  is

$$(P - Q - 1) \cdot (d^{geo}(X_n, X_m) / (d^{geo}(X_i, X_j))),$$

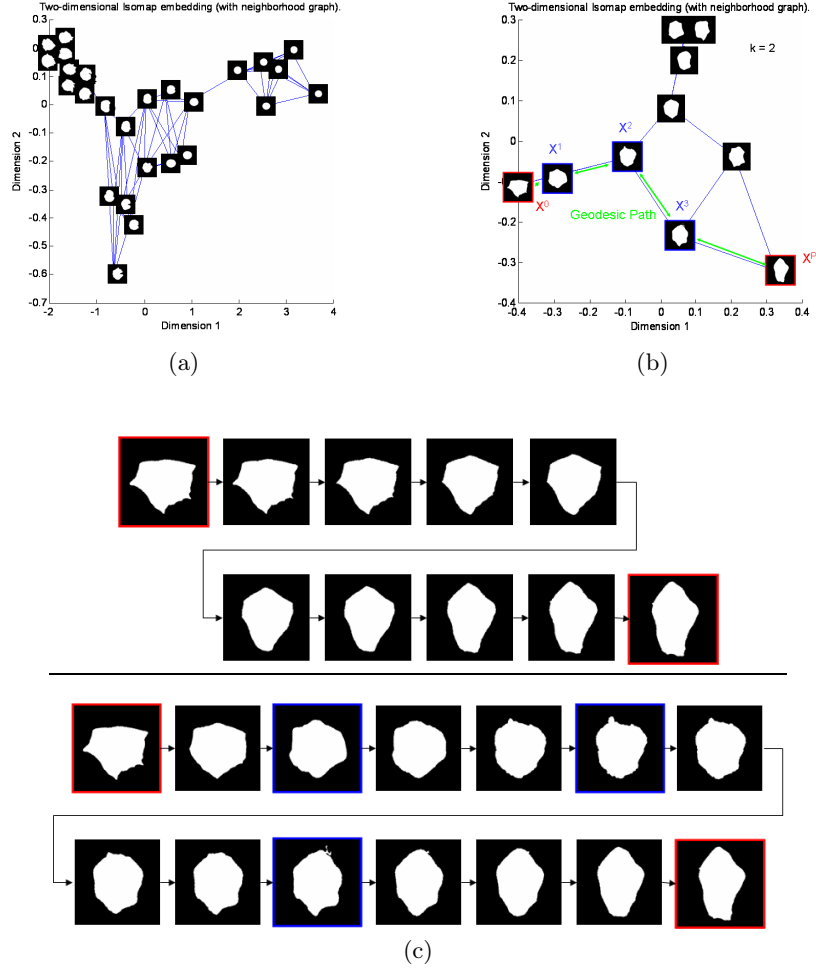


**Fig. 5.** (a) Projection of four populations of shapes on the two first ISOMAP dimensions (using the Jacquard distance). (b) Idem. for family  $\mathcal{X}$ : population B) of Fig. 1(a)). (c) Morphological shape interpolation of 8 intermediate shapes between  $X^0$  and  $X^P$  (in red): Top, interpolation along an Euclidean shape path; bottom, interpolation along a geodesic path (including 3 shapes of the family in blue).

where  $d^{geo}(X, Y)$  is the geodesic distance between the shapes  $X$  and  $Y$ . See example in Fig. 5(c).

Shape interpolation in reduced spaces has been also studied in [5], with a Delaunay triangulation of the training family of shapes in the reduced space. When a new shape  $Y$  is projected in the trained space (which is a difficult problem), the corresponding triangle determines the 3 initial sets which can be used to approach  $Y$  by a barycentric-weighted mean shape. This problem can also be solved in our framework. Let us define the weighting interpolation

function between sets  $X$  and  $Y$  as

$$\text{interp}_X^Y(x; \omega_X, \omega_Y) = \frac{\omega_X d_X^Y(x)}{\omega_X d_X^Y(x) + \omega_Y d_Y^X(x)},$$

where  $\omega_X$  and  $\omega_Y$  are the weights (i.e.,  $\omega_X/\omega_Y$  corresponds to the speed of propagation between sets  $X$  and  $Y$ ). The gravity centre between three sets of the family  $X_i$ ,  $X_j$  and  $X_k$  is obtained as  $X^{i,j,k} = \{x : \text{interp}_{X^{i,j}}^{X_k}(x; 2, 1) \leq 0.5\}$ , where  $X^{i,j} = \{x : \text{interp}_{X_i}^{X_j}(x; 1, 1) \leq 0.5\}$ . The result depends on the processing order however the differences are negligible in practical examples. For the interpolation of a not centred shape in a triangle, the coefficient for each set can be proportionally set up.

## 5 Conclusions

We have proposed efficient tools for analysing shape families using morphological operators. Various algorithms for the computation of mean shape and variance of shape as well as for the construction of shape priors for modes of shape variation have been introduced. We have also illustrated how the morphological interpolation can be used in shape manifolds to obtain more relevant results. The main motivation of this study was to define prototypes and shape targets for model-based morphological segmentation. More generally, the statistical analysis of shapes families requires the computation of advanced notions such as covariance and probability distribution in shape spaces. This last point will be the object of ongoing work.

## References

1. Baddeley, A.J., Molchanov, I.S.: Averaging of Random Sets Based on Their Distance Functions. *Journal of Mathematical Imaging and Vision* 8, 79–92 (1998)
2. Beucher, S.: Sets, partitions and functions interpolations. In: *Mathematical Morphology and its Applications to Image and Signal Processing (Proc. of ISMM 1998)*, pp. 307–314. Kluwer, Dordrecht (1998)
3. Charpiat, G., Faugeras, O., Keriven, R., Maurel, P.: Distance-based shape statistics. In: *IEEE ICAPS 2006*, vol. 5, pp. 925–928 (2006)
4. Delfour, M.C., Zolésio, J.-P.: Shape analysis via orientated distance functions. *J. Funct. Anal.* 123, 129–201 (1994)
5. Etyngier, P., Segonne, F., Keriven, R.: Shape Priors using Manifold Learning Techniques. In: *IEEE ICCV 2007*, pp. 1–8 (2007)
6. Grenander, U.: *General Pattern Theory*. Oxford Univ. Press, Oxford (1993)
7. Horgan, G.W.: Principal Component Analysis of Random Particles. *Journal of Mathematical Imaging and Vision* 12, 169–175 (2000)
8. Jolliffe, I.T.: *Principal Component Analysis*. Springer, New York (1989)
9. Kendall, D.G.: A survey of statistical theory of shape. *Statistical Science* 4, 87–120 (1989)
10. Klassen, E., Srivastava, A., Mio, M., Joshi, S.H.: Analysis of planar shapes using geodesic paths on shape spaces. *IEEE Trans. Pattern Anal. Mach. Intell.* 26(3), 372–383 (2004)

11. Meyer, F.: Morphological interpolation method for mosaic images. In: Mathematical Morphology and its Applications to Image and Signal Processing (Proc. of ISMM 1996). Kluwer, Dordrecht (1996)
12. Meyer, F.: The levelings. In: Mathematical Morphology and its Applications to Image and Signal Processing (Proc. of ISMM 1998), pp. 199–206. Kluwer, Dordrecht (1998)
13. Meyer, F.: L'espace des formes entre 2 formes X et Y. Rapport Technique CMM-Ecole des Mines de Paris, N-/09/MM (2009)
14. Serra, J.: Hausdorff distance and interpolations. In: Mathematical Morphology and its Applications to Image and Signal Processing (Proc. of ISMM 1998), pp. 107–114. Kluwer, Dordrecht (1998)
15. Tenenbaum, J.B., de Silva, V., Langford, J.C.: A Global Geometric Framework for Nonlinear Dimensionality Reduction. *Science* 290, 2319–2323 (2000)
16. Whitaker, R.T.: A Level-Set Approach to Image Blending. *IEEE Trans. Image Proc.* 9(11), 1849–1861 (2000)